NANO LETTERS

pubs.acs.org/NanoLett Letter

# Extended Nucleation and Superfocusing in Colloidal Semiconductor Nanocrystal Synthesis

P. Tim Prins,• Federico Montanarella,• Kim Dümbgen, Yolanda Justo, Johanna C. van der Bok, Stijn O. M. Hinterding, Jaco J. Geuchies, Jorick Maes, Kim De Nolf, Sander Deelen, Hans Meijer, Thomas Zinn, Andrei V. Petukhov, Freddy T. Rabouw, Celso De Mello Donega, Daniel Vanmaekelbergh, and Zeger Hens*

Cite This: *Nano Lett.* 2021, 21, 2487−2496 Read Online

ACCESS | Metrics & More | Article Recommendations | Supporting Information

**ABSTRACT:** Hot-injection synthesis is renowned for producing semiconductor nanocolloids with superb size dispersions. Burst nucleation and diffusion-controlled size focusing during growth have been invoked to rationalize this characteristic yet experimental evidence supporting the pertinence of these concepts is scant. By monitoring a CdSe synthesis *in-situ* with X-ray scattering, we find that nucleation is an extended event that coincides with growth during 15−20% of the reaction time. Moreover, we show that size focusing outpaces predictions of diffusion-limited growth. This observation indicates that nanocrystal growth is dictated by the surface reactivity, which drops sharply for larger nanocrystals. Kinetic reaction simulations confirm that this so-called superfocusing can lengthen the nucleation period and promote size focusing. The finding that narrow size dispersions can emerge from the counteracting effects of extended nucleation and reaction-limited size focusing ushers in an evidence-based perspective that turns hot injection into a rational scheme to produce monodisperse semiconductor nanocolloids.

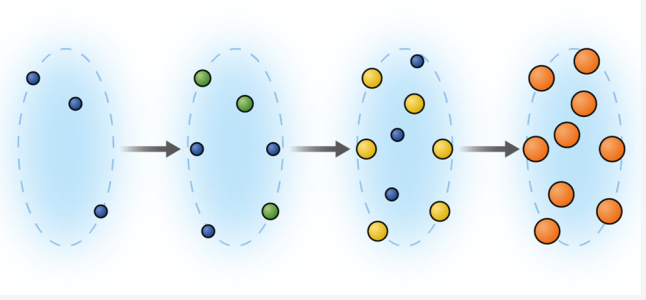

**KEYWORDS:** *nanocolloids, quantum dots, monodisperse, nucleation and growth, in-situ analysis, photoluminescence*

The development of hot-injection synthesis turned colloidal nanocrystals into a widely studied class of nanomaterials with an extensive application potential.[1] The method's central asset is a versatility to produce nanocrystals of very different materials with a variety of morphologies and astonishing precision.[1] The size dispersion (*i.e.*, the ratio between the standard deviation on a characteristic dimension and its mean) can be lower than 5% for the radius $r$ of spherical nanocrystals and zero for the thickness of nanoplatelets.[2] This results in ensembles with optical properties closely resembling those of each individual nanocrystal,[3] which has proven essential for the application of semiconductor nanocrystals in displays,[4,5] lighting,[6,7] photodetection,[8,9] photovoltaics,[10,11] and luminescent solar concentrators.[12,13]

The most-often invoked paradigm to rationalize tight size control by hot injection combines burst nucleation and size focusing.[14−22] Nucleation is then described as a critical process that strongly accelerates above a supersaturation threshold and is quickly arrested by the rapid consumption of the precipitant. As proposed by LaMer *et al.*, the resulting temporal separation of nucleation from growth is what leads to monodisperse colloids.[23] Size focusing refers to the reduction of the standard deviation of the size distribution of a growing nanocrystal ensemble. This absolute focusing happens when small nanocrystals grow faster than large nanocrystals, as is the case for diffusion-limited growth.[24,25] In the case of semiconductor nanocrystal growth, the first observations of size-distribution narrowing were discussed in terms of absolute size focusing.[17,26] Later studies, however, introduced a more relaxed definition of focusing as the reduction of the size dispersion.[27] To attain this relative focusing, a size-independent growth rate, as is often assigned to reaction-limited growth, suffices.[24] Although often invoked and widely accepted, little experimental evidence supports the description of hot injection through burst nucleation and size focusing.[28] Especially for the formation of metal nanoclusters by autocatalytic surface growth, it was claimed that LaMer's paradigm offers little guidance, and alternative synthesis models have been explored.[29−31] However, also in the case of semiconductor nanocrystals, the observation that mono-

**Received:** December 7, 2020
**Revised:** February 18, 2021
**Published:** March 4, 2021

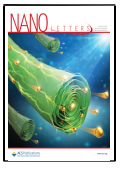

Downloaded via UTRECHT UNIV on June 17, 2021 at 08:33:06 (UTC).
See https://pubs.acs.org/sharingguidelines for options on how to legitimately share published articles.

ACS Publications © 2021 American Chemical Society



https://dx.doi.org/10.1021/acs.nanolett.0c04813
*Nano Lett.* 2021, 21, 2487−2496

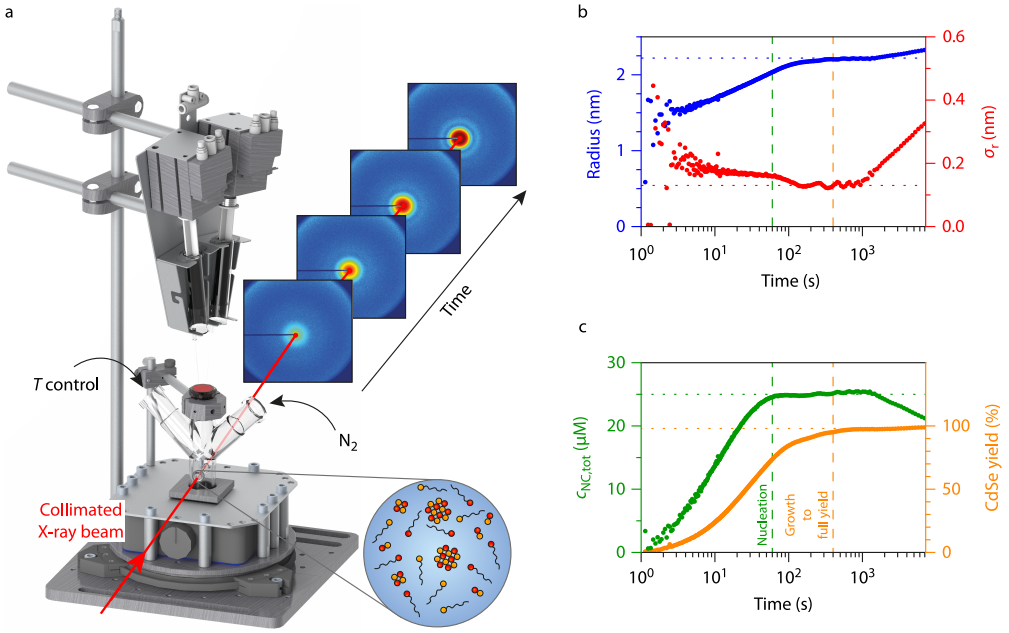


**Figure 1.** *In-situ* time-resolved small-angle X-ray scattering. (a) Schematic of the experimental setup used for *in-situ* monitoring through SAXS of a CdSe hot-injection synthesis based on reacting cadmium oleate with trioctylphosphine selenium. Part of the precursors are loaded into the custom-made three-necked flask, which is heated under a nitrogen atmosphere. The nucleation and growth of the nanocrystals are triggered by the injection of the Cd precursor via the remotely controlled syringe pump placed above the three-necked flask. The reaction is probed with collimated synchrotron-based X-rays through a small indentation in the flask. The 100 ms time resolution of the SAXS detector enables the development of the reaction to be precisely followed. (b) Representation of (blue) the average nanocrystal radius and (red) the standard deviation as a function of reaction time as extracted from successive SAXS patterns (Supporting Information S2). The blue dotted line indicates the final average radius prior to ripening (2.22 nm), and the red dotted line indicates the minimum polydispersity obtained, 0.13 nm (*i.e.*, 6% of the average radius). (c) Representation of (green) the concentration of nanocrystals and (orange) the CdSe yield as a function of reaction time as extracted from successive SAXS patterns (Supporting Information S2). Horizontal dotted lines indicate (green) the nanocrystals' concentration prior to ripening and (orange) the final reaction yield. Vertical dashed lines in b and c indicate the times at which (green) the concentration of nanocrystals and (orange) the yield attain 98% of the final value.

disperse III−V nanocrystals can be formed by continuous precursor injection hints at a more complex mechanism.[32,33]

For the hot-injection synthesis of semiconductor nanocrystals, such as CdSe and PbSe, it was found that the precipitation involves a CdSe[34] or PbSe[35] unit or monomer formed out of the injected metal and chalcogen precursors. Further studies on CdSe,[36,37] PbS,[38] PbSe,[3] InP,[39] and $Cu_2S$[38] showed that the precipitation rate is limited by the precursor to monomer conversion. For such reactions, nucleation and growth become competing pathways of monomer consumption.[36] If the growth rate were zero, then nucleation would continue until monomer generation stopped, which is exactly the opposite from a self-limiting, burst-like event. However, when critical nuclei immediately enter the growth stage, the growth of an increasing number of nanocrystals will lower the supersaturation below the nucleation threshold and arrest nucleation.[36] A central element to understanding the formation of semiconductor nanocrystals by hot-injection synthesis is therefore the rate constant of nanocrystal growth. However, this quantity is unknown, as is the expected nucleation regime in a nanocrystal synthesis.

Here, we analyze nucleation and growth in an established CdSe nanocrystal synthesis.[36,40] Using *in-situ* small-angle X-ray scattering (SAXS) measurements and *ex-situ* absorbance spectroscopy, we show that this synthesis exhibits a prolonged nucleation stage, active during ∼15−20% of the reaction time. Nevertheless, we observe that the size distribution narrows over time (absolute size focusing) such that nanocrystals attain a nearly uniform size when the reaction reaches full yield. Even more, we demonstrate that nanocrystal ensembles with a bimodal size distribution exhibit pronounced size focusing that outpaces diffusion-limited focusing. We assign this finding to a strong drop in surface reactivity with size and confirm through kinetic reaction simulations that such plummeting surface reactivity, a property we call superfocusing, extends the nucleation stage. Under such conditions, narrow size dispersions can result from the counteracting effect of extended nucleation and extreme size focusing.

## EXTENDED NUCLEATION IN HOT-INJECTION SYNTHESIS

We monitored *in-situ* the formation of CdSe nanocrystals from cadmium oleate and trioctylphosphine selenium (Supporting Information S1) through SAXS. We reproduced typical laboratory conditions by using a custom-made setup[41,42] consisting of a three-necked flask equipped with an indentation for X-ray scattering and embedded in a heating mantle with active temperature control (Figure 1a). As described in Supporting Information S1, the necks enabled us to impose a protective atmosphere, measure the temperature, and inject reagents via a remotely controlled syringe pump, an approach complementary to previous studies where reactions were initiated by heating the entire reaction mixture.[43] SAXS patterns were recorded throughout the synthesis, from which we extracted the size and concentration of the nanocrystals as a function of time (Supporting Information S1 and S2).[44] To rule out the possibility of X-ray-induced changes in the


https://dx.doi.org/10.1021/acs.nanolett.0c04813
Nano Lett. 2021, 21, 2487−2496

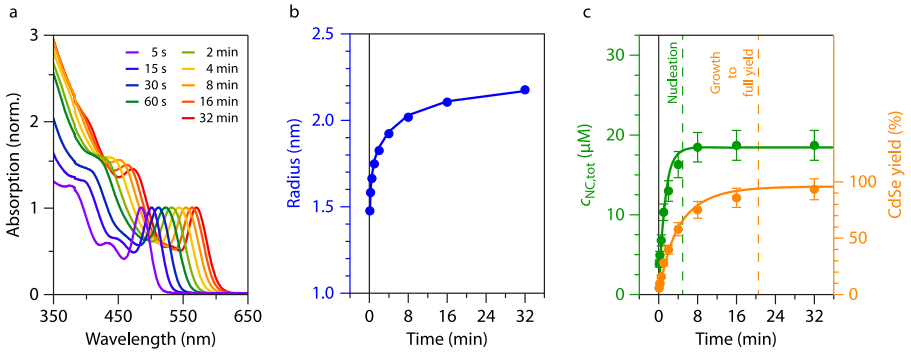


**Figure 2.** Time-resolved optical absorption spectroscopy. (a) Absorbance spectra of reaction aliquots taken as indicated after the start of a CdSe synthesis based on reacting cadmium stearate with trioctylphosphine selenium (details in Supporting Information S3).[36] (b) Nanocrystal radius estimated from the spectral position of the CdSe NC band-edge transition using a SAXS-based sizing curve.[46] (c) (Orange) CdSe yield and (green) concentration of nanocrystals as obtained from the absorbance at 320 nm of quantitative reaction aliquots in combination with the nanocrystal radius. The development of the CdSe yield was fit assuming a second-order monomer generation rate,[36] whereas $c_{NC,tot}$ was fit to an exponential build up (Supporting Information S3). We took the points where the two fits attain 98% of their final value to identify the end of the nucleation and the growth-to-full-yield period as indicated by the green and orange dashed lines, respectively.

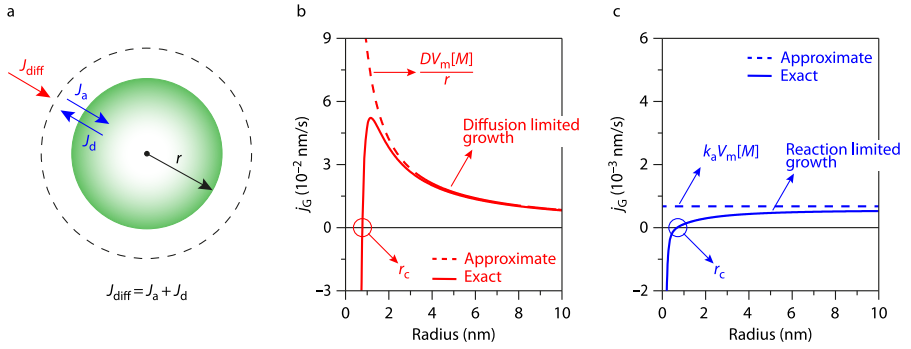


**Figure 3.** Nanocrystal growth rate. (a) Cartoon of a nanocrystal with radius $r$ and the monomer flux by (red) diffusion and (blue) surface reaction leading to nanocrystal growth. (b, c) Representation of the nanocrystal growth rate as a function of $r$ under conditions of (b, red) diffusion-controlled growth and (c, blue) reaction-limited growth. In both cases, the dashed line represents the limiting behavior for large radii used to derive eqs 2 and 3 and $r_c$ indicates the critical radius. See Supporting Information S4 for an overview of the parameters used.

development of the reaction,[45] we performed a similar analysis on the same hot-injection reaction by aliquot-based monitoring (Supporting Information S1).

Figure 1b,c displays the temporal evolution of the average nanocrystal radius $r$ and its standard deviation $\sigma_r$, the yield of CdSe formation, and the nanocrystal concentration $c_{NC,tot}$ as obtained from the *in-situ* SAXS data. Clearly, consistent data analysis is possible after ~3 s of reaction time. As shown in Figure 1b, the CdSe yield reaches 98% within 400 s, a common time span for this type of reaction.[35] This development concurs with a steady increase in radius from ~1.5 to 2.2 nm. More interesting, however, is the observation that the nanocrystal concentration needs 60 s to reach 98% of the final concentration of ~25 μM. This suggests that nucleation persists during 15% of the reaction time. Despite this prolonged nucleation, the size distribution progressively narrows to reach a size dispersion of ~6% after 400 s. Importantly, this evolution involves absolute size focusing, with the standard deviation of the particle size distribution dropping from ~0.18 nm after 10 s to 0.12 nm after 400 s of reaction time. After the CdSe formation is completed, we observe a gradual decrease in the nanocrystal concentration, a slight increase in radius, and a coarsening of the size dispersion, which are three trends characteristic of Ostwald ripening.

We corroborated the *in-situ* SAXS observations by monitoring a CdSe synthesis with a similar precursor chemistry (Supporting Information S3) through the absorbance spectrum of quantitative reaction aliquots.[36] As shown in Figure 2, this study confirmed the prolonged buildup of the nanocrystal concentration. By comparing the moments where $c_{NC,tot}$ and the CdSe yield reach 98% of their final value, we estimate that nucleation continues for about 20% of the reaction time, a number comparable with the outcome of SAXS analysis. A similar conclusion followed from the analysis of reactions forming PbS and CdS nanocrystals, as shown in Supporting Information S3, and has been recently proposed by Karim and co-workers for Pb nanocrystals[30] and by Owen and co-workers for InP nanocrystals.[47] Despite the lack of a single nucleation event distinct from the growth stage, these syntheses yield monodisperse ensembles in agreement with the *in-situ* SAXS study presented in this study. We thus conclude that a prolonged nucleation period is a common feature of hot-injection syntheses, which nevertheless does not prevent such reactions from forming monodisperse nanocrystal sols.

## ■ ANALYZING THE NANOCRYSTAL GROWTH RATES

In line with the LaMer model,[23] many hot-injection syntheses involve a sequential mechanism in which injected precursors first react to form a monomer species that is consumed in a second step by the nucleation of new nanocrystals or the growth of already existing ones.[35−38] This precursor/monomer/nanocrystal sequence was explicitly demonstrated


https://dx.doi.org/10.1021/acs.nanolett.0c04813
Nano Lett. 2021, 21, 2487−2496

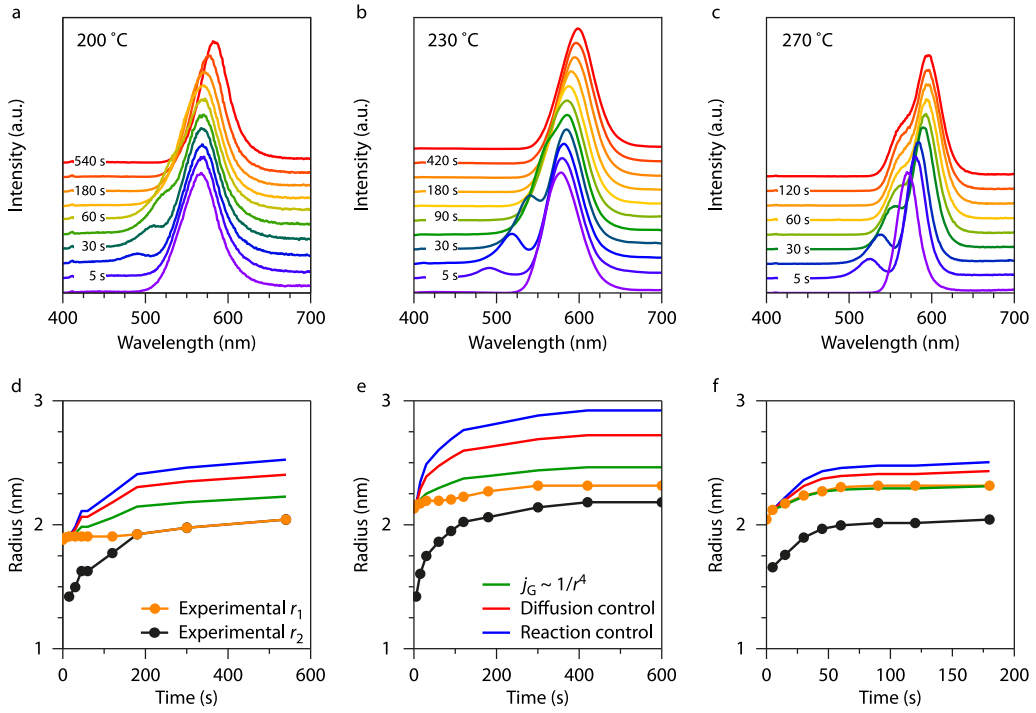


**Figure 4.** Bimodal size distribution experiment. (a–c) Photoluminescence spectra of reaction aliquots taken at the indicated times after the initiation of a second nucleation in a CdSe reaction mixture. The reaction was carried out using chemistry similar to that in Figure 2 at the indicated temperatures. (d–f) Evolution of the radius of (orange dots) the first and (black dots) the second CdSe nanocrystal populations as obtained from the central emission wavelength of both populations. The lines indicate the predicted radius of the first population from the measured radius of the second population assuming (red) diffusion and (blue) reaction control according to eqs 2 and 3, respectively. The green lines in panels d–f represent predicted radii based on a $1/r^4$ scaling of the growth rate (Supporting Information S4).

for the CdSe synthesis analyzed here.[36] Considering that nanocrystal growth involves the diffusion of the monomer to the nanocrystal followed by monomer adsorption at the nanocrystal (Figure 3a), Talapin *et al.* proposed a comprehensive expression for the nanocrystal growth rate $j_G = dr/dt$ (Supporting Information S4):[48]

$$j_G = DV_m[M]_0 \frac{S - S^{r_c/r}}{r + \frac{D}{k_a(r)}} \quad (1)$$

Here, $D$ is the monomer diffusion coefficient, $V_m$ is the material's molar volume, $[M]_0$ is the monomer solubility, $S$ is the supersaturation, $r_c$ is the critical radius, and $k_a(r)$ is the size-dependent rate constant for solute adsorption. Figure 3b,c represents $j_G$ under conditions where diffusion ($D/k_a \ll r$) or surface adsorption ($D/k_a \gg r$) limits growth. According to eq 1, diffusion limitation results in absolute size focusing, while reaction limitation yields a gradually increasing growth rate with nanocrystal size that has the bulk growth rate as an upper limit. This evolution reflects the assumption made in deriving eq 1 that the activation energy for monomer adsorption follows a linear free-energy relation (Supporting Information S4).[48]

The nanocrystal growth regime is important. Absolute size focusing, for example, is often explained by referring to the characteristic $1/r$ scaling of diffusion-limited growth,[14,17,22,25,48] whereas reaction-limited growth may suffice to attain relative size focusing.[27] Because the growth rate depends on two dynamic variables, the nanocrystal radius $r$ and the supersaturation $S$, the actual growth regime cannot be determined by merely following $dr/dt$ during a reaction. This limitation can be overcome by analyzing the evolution of a bimodal size distribution, where different nanocrystal populations grow in a reaction mixture characterized by a single supersaturation, an approach followed before to study Ostwald ripening of CdSe nanocrystals.[49] Under conditions of single supersaturation, radius $r_1$ attained by the first subset in the ensemble can be predicted from radius $r_2$ of the second subset using approximate expressions for growth under diffusion ($j_G \propto S/r$) and reaction ($j_G \propto S$) limitations (Figure 3b,c and Supporting Information S4):

$$r_{1,\text{diffusion}} \approx \sqrt{r_2^2 + (r_{1,0}^2 - r_{2,0}^2)} \quad (2)$$

$$r_{1,\text{reaction}} \approx r_2 + (r_{1,0} - r_{2,0}) \quad (3)$$

Here, $r_{1,0}$ and $r_{2,0}$ indicate the radii of either subset at a given time $t_0$. Hence, comparing experimental radii with predictions based on eqs 2 and 3 provides a straightforward albeit approximate approach to assessing the prevailing growth regime.

## TIME EVOLUTION OF BIMODAL SIZE DISTRIBUTIONS

To create a bimodal size distribution, we initiated a second nucleation event in a reaction mixture by the additional injection of the cadmium precursor during similar CdSe nanocrystal syntheses as discussed in Figure 2, but run using a 10-fold initial excess of TOPSe (Supporting Information S5). We monitored the reaction after the second injection through quantitative aliquots. As shown in Supporting Information S5, this second injection restarts CdSe formation at the same rate as for a single injection and results in a new subset of smaller nanocrystals. As shown in Figure 4a–c, the corresponding bimodal size distribution can be identified in the photo-


https://dx.doi.org/10.1021/acs.nanolett.0c04813
Nano Lett. 2021, 21, 2487–2496

luminescence (PL) spectra of reaction aliquots. These spectra feature a second emission band at shorter wavelength, next to the main PL peak of the initial nanocrystal population, that is not formed without the additional Cd injection (Supporting Information S5).

Deconvolution of the PL spectra using a double Gaussian fit enabled us to determine the wavelength of maximum PL intensity of both subsets, a number from which we estimated the average nanocrystal radius in each subset (Supporting Information S5). The resulting band-edge wavelengths agree with the band-edge absorption of the different subsets, insofar as distinct absorption features can be discerned in the absorption spectra of the aliquots (Supporting Information S5). The resulting radii are represented in Figure 4d–f for the different reaction temperatures, together with predicted radii of the initial subset according to eqs 2 (red, diffusion control) and 3 (blue, reaction control). Remarkably, one sees that at lower temperatures the newly created subset quickly catches up to the initial one. A comparison of the actual and predicted radii makes clear that the larger nanocrystals grow far more slowly than the diffusion-limited and reaction-limited growth predict. This implies that the actual size focusing greatly outpaces the $1/r$ scaling of diffusion-limited growth. This conclusion is supported by the reference line based on a $1/r^4$ scaling of the growth rate, which is reached only for the 270 °C reaction. Importantly, both nanocrystal subsets have the same growth rate once their radii are equal. Hence, the initial sluggish growth of the larger subset is not an artifact due to the poisoning of the CdSe surface during the reaction. We extended this analysis to a different CdSe synthesis, where we used a second injection of black selenium powder to create a bimodal size distribution (Supporting Information S5). For this reaction, both subsets can be clearly identified in the UV–vis absorption spectra of the aliquots, and we again find that the larger subset grows more slowly than the $1/r^4$ reference scaling used in Figure 4.

Whereas little is known as to how the adsorption rate constant $k_a$ changes with the nanocrystal radius, the $1/r$ dependence of diffusion-limited growth is a relation that relies on few assumptions. The monomer diffusion coefficient may decrease with increasing nanocrystal size due to a more pronounced solvent reorganization around larger nanocrystals,[50,51] yet molecular dynamics simulations show such effects to be minor, even at room temperature.[52] Since the growth of the largest subset at the lower temperatures studied (Figure 4a,b) is significantly slower than what diffusion-limited growth predicts, we conclude that growth must be reaction-limited in these cases. Importantly, this implies that $k_a(r)$ must drop more sharply than $1/r$, a situation we will define as superfocusing. Note that this finding is exactly the opposite of what has been argued on the basis of a linear free-energy relation (Figure 3c) and what we implemented in eq 3. Since the growth rate can be expected to increase with temperature more than the diffusion coefficient, higher temperatures can push growth toward diffusion control even for the larger radii, which agrees with our experimental observation at the highest temperature.

## EXTENDED NUCLEATION BY REACTION-LIMITED GROWTH

To understand the impact of superfocusing on the development of a nanocrystal synthesis, we consider the rate $dn_M/dt$ at which a nanocrystal incorporates monomers under reaction-limited growth:

$$\frac{dn_M}{dt} = \frac{1}{V_m}\frac{dV_{NC}}{dt} = 4\pi r^2[M]\frac{k}{r^n} \tag{4}$$

Here, $n_M$ is the number of monomers (in mole) per nanocrystal and $V_{NC}$ is the nanocrystal volume. To explore the impact of superfocusing, we wrote $k_a$ as $k/r^n$and applied eq 1 in the limit of $r \gg r_c$. Note that the units of $k$ in eq 4 change depending on $n$. While this parametrization may seem arbitrary, any growth rate can be approximated around a given $r$ as $k/r^n$ (details in Supporting Information S4). To understand the evolution of [M] when nanocrystals grow larger, we note that $c_{NC,tot}$ will be constant in the absence of nucleation. Since [M] is quasi-stationary,[36] the rate $dn_M/dt$ is also constant when the monomer generation rate is fixed. Under such conditions, $dn_M/dt$ is independent of any time-dependent variable, including radius $r$. Differentiating both sides of eq 4 with respect to $r$, we find that the monomer concentration then changes with radius as

$$\frac{d[M]}{dr} = (n-2)\frac{[M]}{r} \tag{5}$$

Hence, with a growth exponent of $n < 2$, growth concurs with a drop in the monomer concentration. On the other hand, if $n > 2$, the dropping growth rate increases the monomer concentration when nanocrystals grow larger. Note that the former growth regime underpins the LaMer model in which growing nanocrystals quickly arrest nucleation by lowering the supersaturation. In Supporting Information S6, we present a more detailed analysis of the development of a nanocrystal ensemble under the aforementioned conditions. These results confirm that growth at constant monomer generation concurs with a decrease in the supersaturation only when $n < 2$. We thus conclude that when $n > 2$, superfocusing can simultaneously promote size focusing and extend nucleation since growth will fail to reduce the supersaturation below the nucleation threshold for a fixed monomer generation rate.

## KINETIC MODELING UNDER REACTION CONTROL

In a real synthesis, the monomer generation rate decreases with time. To further clarify the relationship between size-focusing and extended nucleation, we ran reaction simulations based on a previously published model in which nucleation is described through classical nucleation theory.[36,53,54] We implemented a reaction scheme in which the injected precursors first react to form the actual precipitate or monomer under pseudo-first-order conditions, a process that applies to the CdSe reaction used here (Supporting Information S6).[34,37] To evaluate the effect of superfocusing on the reaction development, we modeled the rate constant for monomer adsorption as

$$k_a(r) = A\frac{(r_{c,0}+B)^n}{(r+B)^n} \tag{6}$$

Equation 6 is a heuristic model expression in line with the expression proposed in eq 4. Here, small radial offset $B$ avoids the singularity at $r = 0$ and reference radius $r_{c,0}$ provides a convenient way to change the growth exponent while keeping the rate constant fixed at $r_{c,0}$ (Supporting Information S6). As outlined in Supporting Information S4 and S6, we implemented this growth rate to analyze a model synthesis under different focusing conditions. Here, model parameters


https://dx.doi.org/10.1021/acs.nanolett.0c04813
Nano Lett. 2021, 21, 2487–2496

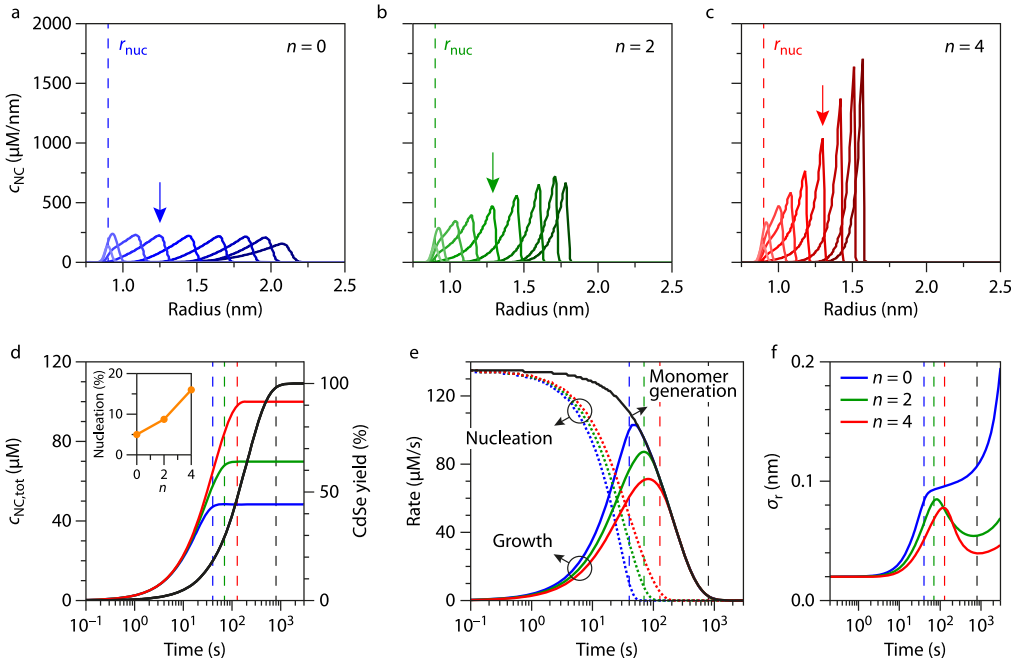


**Figure 5.** Kinetic simulations of nanocrystal growth. (a–c) Snapshots of the nanocrystal distribution $c_{NC}(r)$ at different times in the synthesis as obtained through kinetic reaction simulations. Plots extend from (lightest trace) 3.16 to (darkest trace) 2275 s for growth exponents of (blue) $n$ = 0, (green) 2, and (red) 4. The vertical line indicates the radius at which nanocrystals initially nucleate for the given parameter settings, whereas the arrows highlight the first distribution shown where nucleation has stopped. (d) Time development of the (black) total reaction yield and (colored) total nanocrystal concentration $c_{NC,tot}$ for simulations using different growth exponents as indicated. The vertical lines indicate the moment were (black) the yield and (colored) the nanocrystal concentration attained 98% of the final value. (Inset) Ratio between the time that the concentration and the yield reached 98% of the final value versus the growth exponent. (e) Rates of (black) monomer generation and monomer consumption by (colored dotted lines) nucleation and (colored solid lines) growth for reaction simulations using different growth exponents. (f) Temporal development of the standard deviation of the concentration distribution for reaction simulations with different growth exponents as indicated. The vertical lines in panels e and f have the same meaning as in d.

were chosen in order to have an identical, reaction-limited growth rate at radii close to the critical radius, regardless of the growth exponent, and obtain a reaction development comparable to that in *in-situ* SAXS and *ex-situ* experiments.

Figure 5a–c shows the temporal development of the concentration distribution $c_{NC}(r)$ for three different simulations, where $n$ was set equal to 0, 2 and 4, values that span the presumed range from no superfocusing to superfocusing in agreement with the experimental results shown in Figure 4c. As a compromise between the experimental *in-situ* SAXS and *ex-situ* CdSe synthesis, the simulated syntheses reach a 98% yield after ~800 s (Figure 5d). As shown in Supporting Information S6, the buildup of the nanocrystal concentration we obtain from these simulations closely follows the single-exponential buildup we used to interpolate the experimental data in Figure 2c. Since this outcome also agrees with the *in-situ* SAXS analysis (Supporting Information S6), we conclude that these simulations effectively reproduce the net effect of nucleation, although the molecular aspects of nucleation are not considered.[55] The concentration development plotted in Figure 5d directly shows the impact of superfocusing. All simulated reactions exhibit a nucleation period, characterized by an increasing nanocrystal concentration $c_{NC,tot}$, that gives way to a growth-only regime in which the nanocrystal concentration stays constant. The larger the growth exponent, the longer the nucleation period lasts. The same picture emerges from Figure 5e, where we plotted the contribution of nucleation and growth to the monomer consumption. Comparing the moment at which the concentration and yield reach 98% of their final value shows that the nucleation stage lengthens from 5 to 16% of the reaction time when $n$ increase from 0 to 4. Note that such an extended nucleation is close to the experimental values. We thus conclude that superfocusing can indeed extend the nucleation period to 15% or more of the reaction time.

The concentration distribution snapshots highlight a second aspect of superfocusing. When taking $n$ = 0, growth leads to a mere translation of the concentration distribution once nucleation is stopped. This evolution is expected since a constant $k_a$ makes all nanocrystals grow at the same rate under reaction control.[24] For $n$ = 2 or 4, however, the slower growth rate for larger nanocrystals results in a considerable narrowing of the concentration distribution under conditions of reaction-limited growth. This point is confirmed when we look at the development of the standard deviation $\sigma_r$ of the concentration distribution. While for $n$ = 0, $\sigma_r$ becomes nearly constant once nucleation stops, a clear reduction of $\sigma_r$ is realized during the growth stage when $n$ = 2 or 4, an evolution that reflects absolute focusing of the concentration distribution. We thus conclude that superfocusing can indeed square a circle, extending the nucleation period on the one hand while promoting narrow size distributions on the other hand.

## DISCUSSION

All syntheses analyzed here exhibit a prolonged nucleation period, while size dispersions can be as low as 6%. Such results indicate that in a hot-injection synthesis, burst nucleation is not required to form monodisperse semiconductor nano-


https://dx.doi.org/10.1021/acs.nanolett.0c04813
Nano Lett. 2021, 21, 2487–2496

colloids. Interestingly, such extended nucleation periods have also been reported for the formation of metal nanocrystals through nucleation and surface-catalyzed growth.[29,30] For such reactions, a binary distinction between small, rapidly growing and large, slowly growing nanocrystals was introduced to account for the development of the particle size distribution with time.[31,56] In the precursor-driven synthesis of semiconductor nanocrystals, superfocusing solves in a similar way the paradox between extended nucleation and the formation of monodisperse nanocolloids since the plummeting growth rate strongly focuses the size distribution during reaction-limited growth.

The disappearance of reactive crystal facets is a known principle of crystal growth.[57] Although this concept may explain superfocusing in general terms, it does not provide a concrete, atomistic understanding of the growth process for the materials studied here. Interestingly, recent calculations of the binding energies of cadmium salts to CdSe nanocrystals and nanoplatelets indicated that such ligands bind more weakly to sites near edges than to sites in the center of a crystal facet.[58,59] This difference can promote crystal growth at edges in different ways. First, since such sites are more likely to be free of ligands, monomer addition may be kinetically more favorable, as has been recently argued for the autocatalytic reduction of Pd(II) on Pd nanocrystals.[60] Second, if monomer adsorption involves the breaking of the ligand−nanocrystal bond, then weaker binding sites can thermodynamically favor monomer adsorption. Either way, monomer adsorption will slow down when facets become larger and the fraction of edge sites decreases (*i.e.*, for larger nanocrystals). This effect may be even more pronounced since nucleation on plain facets can be highly unfavorable due to the high edge energy of an initial nucleus formed on such a facet.[61]

While showing that an extended nucleation period can lead to a narrow size distribution, the reaction simulations also yield strongly skewed size distributions with a size dispersion of only 1 to 2%. While such narrow distributions have been reported for the case of PbSe nanocrystals,[3] the *in-situ* SAXS data presented here yielded a larger size dispersion of ∼6%. Hence, the edge of the simulated size distribution at larger radii may especially reflect the limitations of the kinetic model that we implemented. For one thing, we described growth by a single growth exponent $n$, irrespective of the nanocrystal size. In reality, $n$ will tend to zero with increasing size as nanocrystals attain the constant growth rate of the bulk material and the resulting loss of focusing will counteract the development of the steep edge in the size distribution at large radii. However, because the simulations cover a range of radii in which we experimentally observe strong focusing, fixing $n$ at 4 was a conservative choice that leaves little room for adjustments to broaden the size distribution. A more fundamental limitation is implicit in the description of nanocrystals as spheres. Nanocrystals of the same volume can exist in a variety of structures, exposing different facets, edges, and corners. This structural variety precludes a unique relationship between the nanocrystal radius and the growth rate constant and may lead to a growth-rate heterogeneity that diminishes focusing. Understanding such aspects of nanocrystal growth will require atomistic insight into the adsorption and desorption of monomers to nanoscale surfaces.

On the basis of our observations, superfocusing under reaction-limited growth appears to be quite a general mechanism by which monodisperse semiconductor nanocolloids are formed in a hot-injection synthesis. Moreover, because such a mechanism does not require burst nucleation, the same interpretation probably applies to syntheses in which monodisperse nanocolloids are formed by gradually heating up a reaction mixture.[62] Interestingly, the bimodal size distribution reactions shown here highlight that superfocusing can lead to monodisperse nanocolloids despite a most disparate nucleation event, and the conclusion that reaction-limited growth can cause pronounced size-distribution focusing could be put into practice in the design of new colloidal synthesis protocols. Even so, superfocusing can be a double-edged sword. The more strongly the growth rate constant decreases with increasing radius, the longer nucleation persists, which increases the degree of focusing needed to attain a narrow size distribution. This point may explain why the lowest-temperature synthesis shown in Figure 4 exhibits the strongest growth rate decrease but not the best size distributions. Hence, finding the best reaction conditions will remain a matter of careful synthesis optimization. On the other hand, introducing coadsorbents into a reaction to slow down monomer adsorption could be a fruitful strategy for tuning and maximizing the impact of superfocusing. Clearly, this variety of possible strategies already highlights that the concept of superfocusing under reaction control provides a much needed missing link in the mechanistic understanding of nanocolloid synthesis and will prove to be most useful in rationally steering any nanocrystal synthesis to form monodisperse sols.

## ■ ASSOCIATED CONTENT

### Supporting Information

The Supporting Information is available free of charge at https://pubs.acs.org/doi/10.1021/acs.nanolett.0c04813.

*In-situ* analysis by SAXS of a hot-injection synthesis, data analysis of SAXS patterns, aliquot-based reaction development of a PbS and a CdS hot-injection synthesis, description of the nanocrystal growth rate, analysis of the bimodal distribution experiments, and kinetic reaction modeling (PDF)

## ■ AUTHOR INFORMATION


### Corresponding Author

**Zeger Hens** − *Physics and Chemistry of Nanostructures, Ghent University, B-9000 Gent, Belgium;* orcid.org/0000-0002-7041-3375; Email: zeger.hens@ugent.be

### Authors

**P. Tim Prins** − *Debye Institute for Nanomaterials Science, Utrecht University, 3584 CS Utrecht, The Netherlands;* orcid.org/0000-0002-8258-0074

**Federico Montanarella** − *Debye Institute for Nanomaterials Science, Utrecht University, 3584 CS Utrecht, The Netherlands;* orcid.org/0000-0002-9057-7414

**Kim Dümbgen** − *Physics and Chemistry of Nanostructures, Ghent University, B-9000 Gent, Belgium*

**Yolanda Justo** − *Physics and Chemistry of Nanostructures, Ghent University, B-9000 Gent, Belgium*

**Johanna C. van der Bok** − *Debye Institute for Nanomaterials Science, Utrecht University, 3584 CS Utrecht, The Netherlands;* orcid.org/0000-0002-1810-3513

**Stijn O. M. Hinterding** − *Debye Institute for Nanomaterials Science, Utrecht University, 3584 CS Utrecht, The Netherlands;* orcid.org/0000-0002-3940-1253




https://dx.doi.org/10.1021/acs.nanolett.0c04813
*Nano Lett.* 2021, 21, 2487−2496

**Jaco J. Geuchies** − *Debye Institute for Nanomaterials Science, Utrecht University, 3584 CS Utrecht, The Netherlands;* orcid.org/0000-0002-0758-9140
**Jorick Maes** − *Physics and Chemistry of Nanostructures, Ghent University, B-9000 Gent, Belgium;* orcid.org/0000-0002-5666-6544
**Kim De Nolf** − *Physics and Chemistry of Nanostructures, Ghent University, B-9000 Gent, Belgium*
**Sander Deelen** − *Scientific Instrumentation, Faculty of Science, Utrecht University, 3584 CS Utrecht, The Netherlands*
**Hans Meijer** − *Scientific Instrumentation, Faculty of Science, Utrecht University, 3584 CS Utrecht, The Netherlands*
**Thomas Zinn** − *ID02, ESRF, 38000 Grenoble, France*
**Andrei V. Petukhov** − *Debye Institute for Nanomaterials Science, Utrecht University, 3584 CS Utrecht, The Netherlands; Laboratory of Physical Chemistry, Eindhoven University of Technology, 5612 AZ Eindhoven, The Netherlands;* orcid.org/0000-0001-9840-6014
**Freddy T. Rabouw** − *Debye Institute for Nanomaterials Science, Utrecht University, 3584 CS Utrecht, The Netherlands;* orcid.org/0000-0002-4775-0859
**Celso De Mello Donega** − *Debye Institute for Nanomaterials Science, Utrecht University, 3584 CS Utrecht, The Netherlands;* orcid.org/0000-0002-4403-3627
**Daniel Vanmaekelbergh** − *Debye Institute for Nanomaterials Science, Utrecht University, 3584 CS Utrecht, The Netherlands;* orcid.org/0000-0002-3535-8366

Complete contact information is available at: https://pubs.acs.org/10.1021/acs.nanolett.0c04813

### Author Contributions

•P.T.P and F.M. contributed equally to this work. P.T.P and F.M. conceived and designed the SAXS setup and the *in-situ* SAXS experiment, S.D. and J.M. manufactured the SAXS setup, P.T.P., F.M., J.C.V.D.B., S.O.M.H., J.J.G. and A.V.P. performed the SAXS measurements, T.Z. and provided support during the SAXS measurements, P.T.P and F.T.R. analyzed the SAXS data, A.V.P., F.T.R., C.D.M.D. and D.V. supervised the SAXS study, Y.J., J.M. and K.D.N. carried out the aliquot-based syntheses, K.D carried out the kinetic reaction simulations, Z.H. organized the research and wrote the manuscript with input from P.T.P., F.M., K.D, C.D.M.D. and D.V.

### Notes

The authors declare no competing financial interest.

## ■ ACKNOWLEDGMENTS

Z.H. acknowledges support by FWO-Vlaanderen (research projects G0F0920N and G0B2921N) and Ghent University (BOF-GOA 01G01019). K.D. acknowledges FWO-Vlaanderen for a scholarship. Z.H., D.V.M., and F.M. acknowledge support by the European Commission via the Marie-Sklodowska Curie Action Phonsi (H2020-MSCA-ITN-642656). D.V., C.D.M.D., and F.T.R. acknowledge support by The Netherlands Organization for Scientific Research (NWO; grants 14614 "Q-Lumicon", Veni 722.017.002) and The Netherlands Center for Multiscale Catalytic Energy Conversion (MCEC). J.J.G. acknowledges financial support from the joint UU and ESRF Graduate Program. The authors thank the ESRF for providing beam time (experiment HC-3725), Jacques Gorini and Narayanan Theyencheri for assistance during beam time, and Liheng Wu and Matteo Cargnello for fruitful discussions.

## ■ REFERENCES

(1) Kovalenko, M. V.; Manna, L.; Cabot, A.; Hens, Z.; Talapin, D. V.; Kagan, C. R.; Klimov, V. I.; Rogach, A. L.; Reiss, P.; Milliron, D. J.; et al. Prospects of Nanoscience with Nanocrystals. *ACS Nano* **2015**, *9* (2), 1012.
(2) Nasilowski, M.; Mahler, B.; Lhuillier, E.; Ithurria, S.; Dubertret, B. Two-Dimensional Colloidal Nanocrystals. *Chem. Rev.* **2016**, *116* (18), 10934.
(3) Campos, M. P.; Hendricks, M. P.; Beecher, A. N.; Walravens, W.; Swain, R. A.; Cleveland, G. T.; Hens, Z.; Sfeir, M. Y.; Owen, J. S. A Library of Selenourea Precursors to PbSe Nanocrystals with Size Distributions near the Homogeneous Limit. *J. Am. Chem. Soc.* **2017**, *139* (6), 2296.
(4) Bourzac, K. Quantum dots go on display. *Nature* **2013**, *493* (7432), 283.
(5) Luo, Z. Y.; Xu, D. M.; Wu, S. T. Emerging Quantum-Dots-Enhanced LCDs. *J. Disp. Technol.* **2014**, *10* (7), 526.
(6) Shimizu, K. T.; Böhmer, M.; Estrada, D.; Gangwal, S.; Grabowski, S.; Bechtel, H.; Kang, E.; Vampola, K. J.; Chamberlin, D.; Shchekin, O. B.; et al. Toward commercial realization of quantum dot based white light-emitting diodes for general illumination. *Photonics Res.* **2017**, *5* (2), A1.
(7) Shirasaki, Y.; Supran, G. J.; Bawendi, M. G.; Bulovic, V. Emergence of colloidal quantum-dot light-emitting technologies. *Nat. Photonics* **2013**, *7* (1), 13.
(8) Malinowski, P. E.; Georgitzikis, E.; Maes, J.; Vamvaka, I.; Frazzica, F.; Van Olmen, J.; De Moor, P.; Heremans, P.; Hens, Z.; Cheyns, D. Thin-Film Quantum Dot Photodiode for Monolithic Infrared Image Sensors. *Sensors* **2017**, *17* (12), 2867.
(9) Rauch, T.; Boberl, M.; Tedde, S. F.; Furst, J.; Kovalenko, M. V.; Hesser, G. N.; Lemmer, U.; Heiss, W.; Hayden, O. Near-infrared imaging with quantum-dot-sensitized organic photodiodes. *Nat. Photonics* **2009**, *3* (6), 332.
(10) Sun, B.; Voznyy, O.; Tan, H. R.; Stadler, P.; Liu, M. X.; Walters, G.; Proppe, A. H.; Liu, M.; Fan, J.; Zhuang, T. T.; et al. Pseudohalide-Exchanged Quantum Dot Solids Achieve Record Quantum Efficiency in Infrared Photovoltaics. *Adv. Mater.* **2017**, *29* (27), e1700749.
(11) Tang, J.; Kemp, K. W.; Hoogland, S.; Jeong, K. S.; Liu, H.; Levina, L.; Furukawa, M.; Wang, X.; Debnath, R.; Cha, D.; et al. Colloidal-quantum-dot photovoltaics using atomic-ligand passivation. *Nat. Mater.* **2011**, *10* (10), 765.
(12) Meinardi, F.; Colombo, A.; Velizhanin, K. A.; Simonutti, R.; Lorenzon, M.; Beverina, L.; Viswanatha, R.; Klimov, V. I.; Brovelli, S. Large-area luminescent solar concentrators based on 'Stokes-shift-engineered' nanocrystals in a mass-polymerized PMMA matrix. *Nat. Photonics* **2014**, *8* (5), 392.
(13) Wu, K.; Li, H.; Klimov, V. I. Tandem luminescent solar concentrators based on engineered quantum dots. *Nat. Photonics* **2018**, *12* (2), 105.
(14) Kwon, S. G.; Hyeon, T. Formation Mechanisms of Uniform Nanocrystals via Hot-Injection and Heat-Up Methods. *Small* **2011**, *7* (19), 2685.
(15) Park, J.; Joo, J.; Kwon, S. G.; Jang, Y.; Hyeon, T. Synthesis of monodisperse spherical nanocrystals. *Angew. Chem., Int. Ed.* **2007**, *46* (25), 4630.
(16) Sugimoto, T. Preparation of Monodispersed Colloidal Particles. *Adv. Colloid Interface Sci.* **1987**, *28* (1), 65.
(17) Yin, Y.; Alivisatos, A. P. Colloidal nanocrystal synthesis and the organic-inorganic interface. *Nature* **2005**, *437* (7059), 664.
(18) Murray, C. B.; Kagan, C. R.; Bawendi, M. G. Synthesis and characterization of monodisperse nanocrystals and close-packed nanocrystal assemblies. *Annu. Rev. Mater. Sci.* **2000**, *30*, 545.
(19) Reiss, P.; Carrière, M.; Lincheneau, C.; Vaure, L.; Tamang, S. Synthesis of Semiconductor Nanocrystals, Focusing on Nontoxic and Earth-Abundant Materials. *Chem. Rev.* **2016**, *116* (18), 10731.
(20) Thanh, N. T. K.; Maclean, N.; Mahiddine, S. Mechanisms of Nucleation and Growth of Nanoparticles in Solution. *Chem. Rev.* **2014**, *114* (15), 7610.

(21) Wang, Y.; He, J.; Liu, C.; Chong, W. H.; Chen, H. Thermodynamics versus Kinetics in Nanosynthesis. *Angew. Chem., Int. Ed.* **2015**, *54* (7), 2022.
(22) Bullen, C. R.; Mulvaney, P. Nucleation and growth kinetics of CdSe nanocrystals in octadecene. *Nano Lett.* **2004**, *4* (12), 2303.
(23) LaMer, V. K.; Dinegar, R. H. Theory, Production and Mechanism of Formation of Monodispersed Hydrosols. *J. Am. Chem. Soc.* **1950**, *72* (11), 4847.
(24) Dirksen, J. A.; Ring, T. A. Fundamentals of crystallization: Kinetic effects on particle size distributions and morphology. *Chem. Eng. Sci.* **1991**, *46* (10), 2389.
(25) Reiss, H. The Growth of Uniform Colloidal Dispersions. *J. Chem. Phys.* **1951**, *19* (4), 482.
(26) Peng, X. G.; Wickham, J.; Alivisatos, A. P. Kinetics of II-VI and III-V colloidal semiconductor nanocrystal growth: "Focusing" of size distributions. *J. Am. Chem. Soc.* **1998**, *120* (21), 5343.
(27) Rempel, J. Y.; Bawendi, M. G.; Jensen, K. F. Insights into the Kinetics of Semiconductor Nanocrystal Nucleation and Growth. *J. Am. Chem. Soc.* **2009**, *131* (12), 4479.
(28) Whitehead, C. B.; Özkar, S.; Finke, R. G. LaMer's 1950 model of particle formation: a review and critical analysis of its classical nucleation and fluctuation theory basis, of competing models and mechanisms for phase-changes and particle formation, and then of its application to silver halide, semiconductor, metal, and metal-oxide nanoparticles. *Materials Advances* **2021**, *2* (1), 186.
(29) Watzky, M. A.; Finke, R. G. Transition metal nanocluster formation kinetic and mechanistic studies. A new mechanism when hydrogen is the reductant: Slow, continuous nucleation and fast autocatalytic surface growth. *J. Am. Chem. Soc.* **1997**, *119* (43), 10382.
(30) Mozaffari, S.; Li, W.; Thompson, C.; Ivanov, S.; Seifert, S.; Lee, B.; Kovarik, L.; Karim, A. M. Colloidal nanoparticle size control: experimental and kinetic modeling investigation of the ligand−metal binding role in controlling the nucleation and growth kinetics. *Nanoscale* **2017**, *9* (36), 13772.
(31) Handwerk, D. R.; Shipman, P. D.; Whitehead, C. B.; Özkar, S.; Finke, R. G. Mechanism-Enabled Population Balance Modeling of Particle Formation en Route to Particle Average Size and Size Distribution Understanding and Control. *J. Am. Chem. Soc.* **2019**, *141* (40), 15827.
(32) Franke, D.; Harris, D. K.; Chen, O.; Bruns, O. T.; Carr, J. A.; Wilson, M. W. B.; Bawendi, M. G. Continuous injection synthesis of indium arsenide quantum dots emissive in the short-wavelength infrared. *Nat. Commun.* **2016**, *7*, 12749.
(33) Achorn, O. B.; Franke, D.; Bawendi, M. G. Seedless Continuous Injection Synthesis of Indium Phosphide Quantum Dots as a Route to Large Size and Low Size Dispersity. *Chem. Mater.* **2020**, *32* (15), 6532.
(34) Liu, H. T.; Owen, J. S.; Alivisatos, A. P. Mechanistic study of precursor evolution in colloidal group II-VI semiconductor nanocrystal synthesis. *J. Am. Chem. Soc.* **2007**, *129* (2), 305.
(35) Steckel, J. S.; Yen, B. K. H.; Oertel, D. C.; Bawendi, M. G. On the mechanism of lead chalcogenide nanocrystal formation. *J. Am. Chem. Soc.* **2006**, *128* (40), 13032.
(36) Abe, S.; Capek, R. K.; De Geyter, B.; Hens, Z. Tuning the Postfocused Size of Colloidal Nanocrystals by the Reaction Rate: From Theory to Application. *ACS Nano* **2012**, *6*, 42.
(37) Owen, J. S.; Chan, E. M.; Liu, H.; Alivisatos, A. P. Precursor Conversion Kinetics and the Nucleation of Cadmium Selenide Nanocrystals. *J. Am. Chem. Soc.* **2010**, *132* (51), 18206.
(38) Hendricks, M. P.; Campos, M. P.; Cleveland, G. T.; Jen-La Plante, I.; Owen, J. S. A tunable library of substituted thiourea precursors to metal sulfide nanocrystals. *Science* **2015**, *348* (6240), 1226.
(39) Tessier, M. D.; Dupont, D.; De Nolf, K.; De Roo, J.; Hens, Z. Economic and Size-Tunable Synthesis of InP/ZnE (E = S, Se) Colloidal Quantum Dots. *Chem. Mater.* **2015**, *27* (13), 4893.
(40) Qu, L. H.; Peng, Z. A.; Peng, X. G. Alternative routes toward high quality CdSe nanocrystals. *Nano Lett.* **2001**, *1* (6), 333.
(41) Wu, L. H.; Fournier, A. P.; Willis, J. J.; Cargnello, M.; Tassone, C. J. In Situ X-ray Scattering Guides the Synthesis of Uniform PtSn Nanocrystals. *Nano Lett.* **2018**, *18* (6), 4053.
(42) Wu, L. H.; Willis, J. J.; McKay, I. S.; Diroll, B. T.; Qin, J.; Cargnello, M.; Tassone, C. J. High-temperature crystallization of nanocrystals into three-dimensional superlattices. *Nature* **2017**, *548* (7666), 197.
(43) Abecassis, B.; Bouet, C.; Garnero, C.; Constantin, D.; Lequeux, N.; Ithurria, S.; Dubertret, B.; Pauw, B. R.; Pontoni, D. Real-Time in Situ Probing of High-Temperature Quantum Dots Solution Synthesis. *Nano Lett.* **2015**, *15* (4), 2620.
(44) Narayanan, T.; Sztucki, M.; Van Vaerenbergh, P.; Leonardon, J.; Gorini, J.; Claustre, L.; Sever, F.; Morse, J.; Boesecke, P. A multipurpose instrument for time-resolved ultra-small-angle and coherent X-ray scattering. *J. Appl. Crystallogr.* **2018**, *51*, 1511.
(45) Flores-Rojas, G. G.; López-Saucedo, F.; Bucio, E. Gamma-irradiation applied in the synthesis of metallic and organic nanoparticles: A short review. *Radiat. Phys. Chem.* **2020**, *169*, 107962.
(46) Maes, J.; Castro, N.; De Nolf, K.; Walravens, W.; Abécassis, B.; Hens, Z. Size and Concentration Determination of Colloidal Nanocrystals by Small-Angle X-ray Scattering. *Chem. Mater.* **2018**, *30* (12), 3952.
(47) McMurtry, B. M.; Qan, K.; Teglasi, J. K.; Swarnakar, A. K.; De Roo, J.; Owen, J. S. Continuous Nucleation and Size Dependent Growth Kinetics of Indium Phosphide Nanocrystals. *Chem. Mater.* **2020**, *32* (10), 4358.
(48) Talapin, D. V.; Rogach, A. L.; Haase, M.; Weller, H. Evolution of an Ensemble of Nanoparticles in a Colloidal Solution: Theoretical Study. *J. Phys. Chem. B* **2001**, *105*, 12278.
(49) Thessing, J.; Qian, J.; Chen, H.; Pradhan, N.; Peng, X. Interparticle Influence on Size/Size Distribution Evolution of Nanocrystals. *J. Am. Chem. Soc.* **2007**, *129* (10), 2736.
(50) Thoma, S. L. J.; Krauss, S. W.; Eckardt, M.; Chater, P.; Zobel, M. Atomic insight into hydration shells around facetted nanoparticles. *Nat. Commun.* **2019**, *10*, 995.
(51) Zobel, M.; Neder, R. B.; Kimber, S. A. J. Universal solvent restructuring induced by colloidal nanoparticles. *Science* **2015**, *347* (6219), 292.
(52) Spagnoli, D.; Gilbert, B.; Waychunas, G. A.; Banfield, J. F. Prediction of the effects of size and morphology on the structure of water around hematite nanoparticles. *Geochim. Cosmochim. Acta* **2009**, *73* (14), 4023.
(53) Kwon, S. G.; Piao, Y.; Park, J.; Angappane, S.; Jo, Y.; Hwang, N.-M.; Park, J.-G.; Hyeon, T. Kinetics of Monodisperse Iron Oxide Nanocrystal Formation by "Heating-Up" Process. *J. Am. Chem. Soc.* **2007**, *129*, 12571.
(54) Vetter, T.; Iggland, M.; Ochsenbein, D. R.; Hänseler, F. S.; Mazzotti, M. Modeling Nucleation, Growth, and Ostwald Ripening in Crystallization Processes: A Comparison between Population Balance and Kinetic Rate Equation. *Cryst. Growth Des.* **2013**, *13* (11), 4890.
(55) Bojesen, E. D.; Iversen, B. B. The chemistry of nucleation. *CrystEngComm* **2016**, *18* (43), 8332.
(56) Handwerk, D. R.; Shipman, P. D.; Whitehead, C. B.; Özkar, S.; Finke, R. G. Particle Size Distributions via Mechanism-Enabled Population Balance Modeling. *J. Phys. Chem. C* **2020**, *124* (8), 4852.
(57) Berti, D.; Palazzo, G. *Colloidal Foundations of Nanoscience*; Elsevier: Amsterdam, 2014.
(58) Singh, S.; Tomar, R.; ten Brinck, S.; De Roo, J.; Geiregat, P.; Martins, J. C.; Infante, I.; Hens, Z. Colloidal CdSe Nanoplatelets, A Model for Surface Chemistry/Optoelectronic Property Relations in Semiconductor Nanocrystals. *J. Am. Chem. Soc.* **2018**, *140* (41), 13292.
(59) Drijvers, E.; De Roo, J.; Martins, J. C.; Infante, I.; Hens, Z. Ligand Displacement Exposes Binding Site Heterogeneity on CdSe Nanocrystal Surfaces. *Chem. Mater.* **2018**, *30* (3), 1178.
(60) Mozaffari, S.; Li, W. H.; Dixit, M.; Seifert, S.; Lee, B.; Kovarik, L.; Mpourmpakis, G.; Karim, A. M. The Role of Nanoparticle Size and Ligand Coverage in Size Focusing of Colloidal Metal Nanoparticles. *Nanoscale Adv.* **2019**, *1* (10), 4052.


https://dx.doi.org/10.1021/acs.nanolett.0c04813
*Nano Lett.* 2021, 21, 2487−2496

(61) Riedinger, A.; Ott, F. D.; Mule, A.; Mazzotti, S.; Knüsel, P. N.; Kress; Stephan, J. P.; Prins, F.; Erwin, S. C.; Norris, D. J. An intrinsic growth instability in isotropic materials leads to quasi-two-dimensional nanoplatelets. *Nat. Mater.* **2017**, *16*, 743.
(62) van Embden, J.; Chesman, A. S. R.; Jasieniak, J. J. The Heat-Up Synthesis of Colloidal Nanocrystals. *Chem. Mater.* **2015**, *27* (7), 2246.



https://dx.doi.org/10.1021/acs.nanolett.0c04813
*Nano Lett.* 2021, 21, 2487−2496